The Extra-Pathway Interactome of the TCA Cycle: Expected and Unexpected Metabolic Interactions[1][OPEN]

Youjun Zhang,[a] Corné Swart,[a] Saleh Alseekh,[a] Federico Scossa,[a,b] Liang Jiang,[a] Toshihiro Obata,[a] Alexander Graf,[a] and Alisdair R. Fernie[a,2]

[a]Max-Planck-Institut für Molekulare Pflanzenphysiologie, 14476 Potsdam-Golm, Germany
[b]Consiglio per la Ricerca in Agricoltura e l'Analisi dell'Economia Agraria, 00134 Rome, Italy

ORCID IDs: 0000-0003-1052-0256 (Y.Z.); 0000-0003-2067-5235 (S.A.); 0000-0002-6233-1679 (F.S.); 0000-0001-8931-7722 (T.O.); 0000-0002-6696-5206 (A.G.); 0000-0001-9000-335X (A.R.F.) (A.R.F.)

The plant tricarboxylic acid (TCA) cycle provides essential precursors for respiration, amino acid biosynthesis, and general nitrogen metabolism; moreover, it is closely involved in biotic stress responses and cellular redox homeostasis. To further understand the in vivo function of the TCA cycle enzymes, we combined affinity purification with proteomics to generate a comprehensive extra-pathway protein-protein interaction network of the plant TCA cycle. We identified 125 extra-pathway interactions in Arabidopsis (*Arabidopsis thaliana*) mostly related to the mitochondrial electron transport complex/ATP synthesis and amino acid metabolism but also to proteins associated with redox stress. We chose three high-scoring and two low-scoring interactions for complementary bimolecular fluorescence complementation and yeast two-hybrid assays, which highlighted the reliability of our approach, supported the intimate involvement of TCA cycle enzymes within many biological processes, and reflected metabolic changes reported previously for the corresponding mutant lines. To analyze the function of a subset of these interactions, we selected two mutants of mitochondrial glutaredoxin S15 and Amidase, which have not yet been analyzed with respect to their TCA cycle function, and performed metabolite profiling and flux analysis. Consistent with their interactions identified in this study, TCA cycle metabolites and the relative TCA flux of the two mutants were altered significantly.

Protein interactions of (sequential) enzymes, so called metabolons (Srere, 1985), play an important role in metabolic regulation (Winkel, 2004; Graham et al., 2007). In plants, a wide range of metabolons have been postulated, including those in glycolysis, the tricarboxylic acid (TCA) cycle, the mitochondrial electron transport chain, photosynthesis, polyamine biosynthesis, and a range of secondary metabolic pathways, including cyanogenic glucoside, phenylpropanoid, and opiate synthesis (Panicot et al., 2002; Giegé et al., 2003; Jørgensen et al., 2005; Shen, 2015; Winzer et al., 2015; Laursen et al., 2016; Zhang et al., 2017a). Early studies on assemblies of metabolic enzymes were carried out, since a discord was observed between pathway activities and the abundance of metabolic intermediates, which could not be explained if the pathways were not subject to some kind of organizational structure (Srere, 1987). To address this, Srere et al. (1973) demonstrated that an immobilized pairing of malate dehydrogenase and citrate synthase showed a kinetic advantage over the free enzymes. A variety of other early experiments using a combination of electron microscopy, cross-linking, biochemistry, and calculations on the basis of stereomorphological measurements of mitochondria (Srere, 1987) further supported the concept of organization of the TCA cycle enzymes that Srere (1985) termed the metabolon. Since these pioneering studies, considerable advances have been made in both cell biological and proteomic approaches that have resulted in the identification of a wide range of protein-protein interactions between consecutive (and also nonconsecutive) pathway enzymes.

In the process of characterizing the intra-TCA cycle interactome, we uncovered functional TCA cycle metabolons in plants by combining protein-protein interaction studies and isotope dilution experiments (Zhang et al., 2017a). Various advantages of plant metabolons have been postulated, including local enrichment of metabolites to achieve a high reaction rate, isolation of intermediates from competing reactions, protection of unstable intermediates, and sequestration of cytotoxic metabolites. The plant TCA cycle is a crucial component of respiratory metabolism, primarily linking the products of the oxidation of pyruvate and malate to CO_2 with the generation of NADH for oxidation by

[1]This work was supported by funding from the Max Planck Society (A.G., T.O., A.R.F.), from the Deutsche Forschungsgemeinschaft (OB 438/1-1 to T.O.), from the German Academic Exchange Service (Deutsche Akademische Austauschdienst Dienst; Y.Z.), and by the International Max Planck Research Schools PhD program (Y.Z.).

[2]Address correspondence to fernie@mpimp-golm.mpg.de.

The author responsible for distribution of materials integral to the findings presented in this article in accordance with the policy described in the Instructions for Authors (www.plantphysiol.org) is: Alisdair Fernie (fernie@mpimp-golm.mpg.de).

Y.Z., T.O., and A.R.F. designed the experiments; Y.Z. performed cDNA cloning and vector construction and developed and conducted protein-protein interaction assays; Y.Z. and L.J. performed T-DNA identification and GC-MS; Y.Z. and S.A. performed the ^{14}C-labeling experiment; Y.Z., C.S., and A.G. performed the LC-MS/MS analysis; F.S. performed the bioinformatics analysis; Y.Z. and A.R.F. wrote the article.

[OPEN]Articles can be viewed without a subscription.
www.plantphysiol.org/cgi/doi/10.1104/pp.17.01687

the mitochondrial electron transport complex (mETC; Nunes-Nesi et al., 2013). The regulation of the plant TCA cycle has been well characterized at a range of levels, including historical kinetic studies, transcriptional and proteomic studies, and, most recently, identification of intra-pathway protein-protein interactions (Nunes-Nesi et al., 2013; Zhang et al., 2017a). In addition, the TCA cycle often operates in noncyclic flux modes, for example, in leaves in the light, in some developing oilseeds, and under specific physiological conditions such as anoxia (Gauthier et al., 2010; Sweetlove et al., 2010). In such instances, it seems likely that the pathway largely fulfills other roles, such as the provision of carbon skeletons for amino acid metabolism or roles in nitrogen metabolism, biotic stress responses, and the optimization of photosynthesis and plant cell redox homeostasis (Araújo et al., 2012). Given that affinity purification-mass spectrometry (AP-MS) experiments are widely used to generate meaningful interaction networks (Puig et al., 2001; Bürckstümmer et al., 2006; Morris et al., 2014; Zhang et al., 2017a), it follows that they could be used to produce information-rich data concerning extra-pathway protein-protein interactions. Such interactions could aid in the characterization of the functions of the interacting proteins, provide detailed catalogs of proteins involved in protein complexes and biological processes, and reveal networks of biological processes at local and proteome-wide scales (Morris et al., 2014). Here, we identified 125 interactions between subunits of TCA cycle enzymes and proteins associated with other pathways. These interactions confirm the previously identified pathway interconnections and open up new avenues for future study.

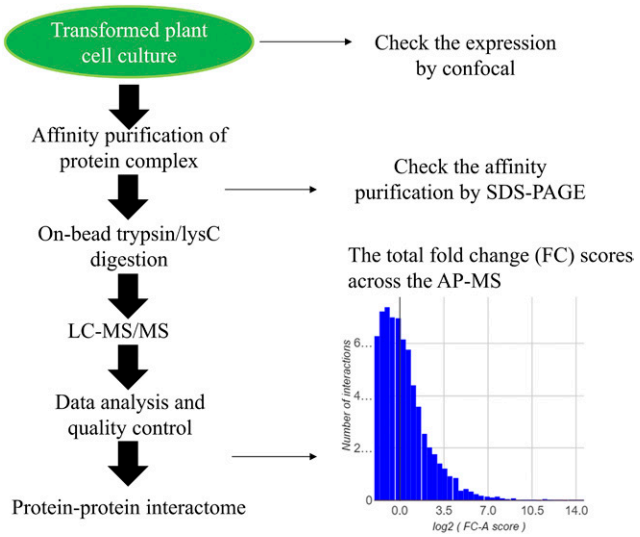

Figure 1. Work flow of the on-bead trypsin/LysC digestion method for AP-MS analysis of protein-protein interaction. The bait was expressed in plant cell culture and checked by confocal microscopy. Following affinity purification using a GFP-binding protein (GFP-Trap; ChromoTek), the protein complexes were digested on beads followed by label-free liquid chromatography (LC)-MS/MS quantification. The intensities of proteomics were analyzed by CRAPome to get the FC score.

RESULTS

Utilization of a Modified AP-MS Protocol to Investigate the Extra-Pathway Protein-Protein Interaction Network of the TCA Cycle

The 38 mitochondrial proteins of Arabidopsis (*Arabidopsis thaliana*) were transformed into the PSB-D Arabidopsis plant cell culture, and a GFP tag-based modified AP-MS procedure was implemented based on at least three biological replicates (Fig. 1). AP-MS has become the method of choice for discovering protein-protein interactions under native conditions. The success of AP-MS depends on the efficiency of trypsin digestion and the recovery of the tryptic peptides for MS analysis (Zhang et al., 2017b). Unlike normal AP-MS, in which the gel is cut into pieces for several independent trypsin digestions (Morris et al., 2014), we used a proteomics-based, in-solution digestion method to directly digest the proteins on the beads following affinity purification (Fig. 1; Supplemental Fig. S1; Zhang et al., 2017b). Thus, an AP-MS experiment constitutes a single sample for the LC-MS measurement (Fig. 1). In the subsequent data analysis, normalized signal intensities were processed to determine fold change abundance (FC-A) scores using the SAINT algorithm embedded within the CRAPome software (Choi et al., 2012; Morris et al., 2014). A total of 3,421 protein-protein interactions were obtained displaying in excess of 4-fold changes in the five independent experiments (Supplemental Table S1). We considered only the protein pairs for which the scores were in the top 10%, corresponding to FC-A values of at least four within at least three of the replicates as positive interactions. A total of 449 potential positive protein-protein interactions were obtained following these criteria, including those interactions with several ribosomal and protein translation proteins (Supplemental Table S2).

As we were interested exclusively in the mitochondrial interactions, we selected only the mitochondria-targeted proteins for generating the network. It is important to note that, given that many of the enzymes of the TCA cycle have isoforms (exhibiting high sequence similarity) in more than one compartment, the nonmitochondrial interactions, while not directly physiologically relevant, may provide hints to interactions that occur in vivo, albeit extra-mitochondrially. Screening of the SUBA4 database (Hooper et al., 2017) revealed a total of 257 interactions between mitochondrially localized TCA cycle proteins and 37 target proteins to comprise our mitochondrial interaction network (Supplemental Table S3). Of these 257 interactions, 132 interactions between the enzymes of the TCA cycle were already reported (Zhang et al., 2017a), while we identified 125 novel interactions between subunits of enzymes and other pathway enzymes or proteins

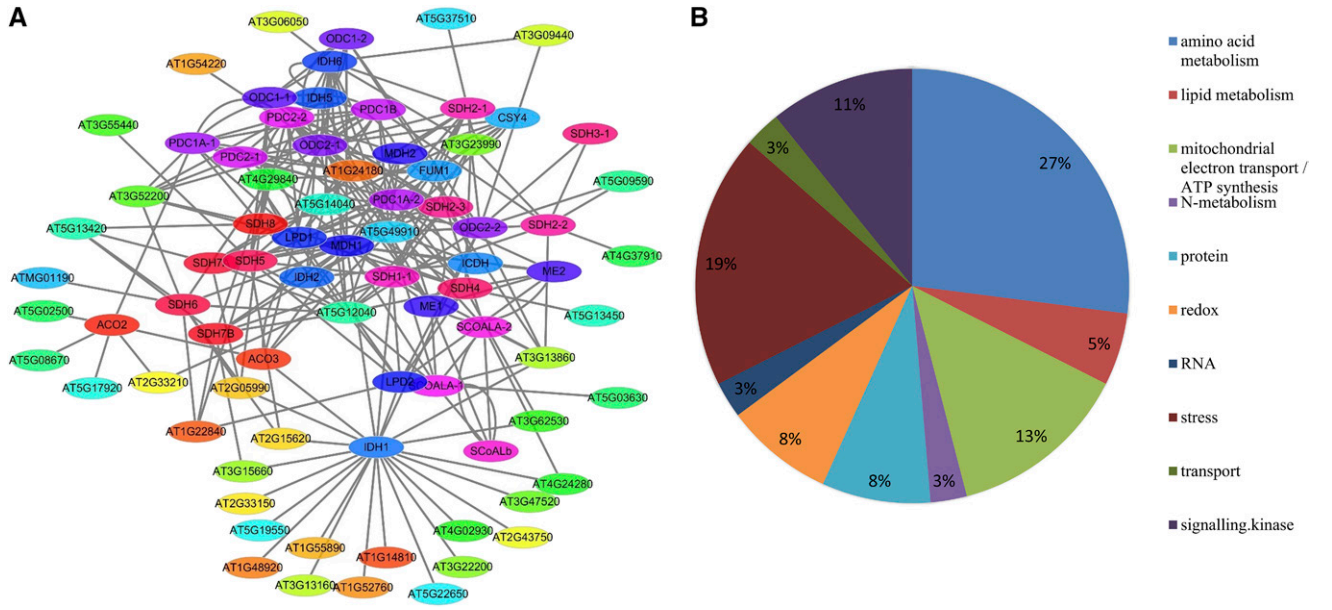

Figure 2. Graphical representation of the protein-protein interaction network of Arabidopsis TCA cycle enzymes. Node color represents the enzyme subunits and isoforms. A, Overview of all detected 257 interactions, including 132 interactions between the enzymes of the TCA cycle and 125 novel interactions between subunits of enzymes and other pathway enzymes or proteins. B, Classification of all 37 preys with molecular function. Ten groups of preys were detected by affinity purification, with large ratios of 27% amino acid metabolism, 19% stress, 13% mitochondrial electron transport/ATP synthesis, and 8% redox.

(Fig. 2A; Table I; Supplemental Fig. S2). On the basis of the functions of these 37 prey proteins (which was assessed by MAPMAN classification; Thimm et al., 2004), we classified the novel 125 interactions into 11 groups (Fig. 2B; Table I; Supplemental Table S4), most of them being related to amino acid metabolism (27%), mETC/ATP synthesis (13%), signaling (11%), lipid metabolism (5%), nitrogen metabolism (3%), and stress (19%). We also checked whether the transcripts encoding each partner of our 125 protein-protein interactions showed evidence of correlation by surveying coexpression databases (ATTED-II, http://atted.jp/; Obayashi et al., 2018), which contain Arabidopsis coexpression data gathered from a number of different transcriptomics data sets. The results of this survey are presented in Table I. A minor fraction of our protein-protein interactions also show transcript coexpression, which is not surprising, as regulation of enzymes is often achieved by a range of different posttranslational mechanisms, as is the case for several enzymes of the TCA cycle, but not through changes in the expression of their encoding genes (Araújo et al., 2012).

Identification of Selected Interaction Pairs by Yeast Two-Hybrid Assays and Bimolecular Fluorescence Complementation

As the FC score of the AP-MS analysis is indicative of the interaction intensity (Mellacheruvu et al., 2013), we next selected three high-FC-scoring protein interactions and two low-scoring interactions for analyzing the protein interaction network (Fig. 3A). Here, we used yeast two-hybrid (Y2H) assays and complementary bimolecular fluorescence complementation (BiFC) assays to analyze binary protein interactions (Fig. 3). For the Y2H assays, protein pairs for which colonies were observed at 3 d post inoculation were regarded as positive interactions. The interaction between Succinate Dehydrogenase5 (SDH5) and Threonine Synthase was not detected via the Y2H assay, most likely due to the fact that SDH5 is a membrane-bound protein, while all other paired interactions were confirmed, particularly notable being the strong interaction between Isocitrate Dehydrogenase (IDH1) and Mitochondrial Glutaredoxin S15 (GRXS15; Fig. 3B). Furthermore, these interactions were all validated independently by BiFC assays, which enable qualitative but highly sensitive detection of protein-protein interactions with subcellular localization information (Fig. 3C; Gehl et al., 2009; Zhang et al., 2017a). Importantly, no BiFC signal was detected for any of the enzyme pairs that were not defined in our AP-MS interaction network.

Analysis of the Metabolism of Select Mutants

To further analyze these interactions, we selected a published knockdown mutant of *GRXS15* (Salk_112767; Ströher et al., 2016) and the *amidase* knockout mutant (Sail_608_A02; Zhang and Marsolais, 2014) and performed metabolite profiling (Fig. 4; Supplemental Table S5) on them in comparison with their wild-type controls. We identified 62 primary metabolites

Table I. The 125 extra-pathway interactions

Bait	Bait AGI Code	Prey[a]	FC-A	Predicted Interaction in Complexome Map[b]	Coexpression (ATTED-II) and Mutual Rank and Occurrence in the First 500 Neighbors[c]
ACO2	AT4G26970	AT2G33210	4. 2	No	No
ACO2	AT4G26970	AT5G02500	7.9	Yes	No
ACO2	AT4G26970	AT5G08670	6.6	Yes	No
ACO2	AT4G26970	AT5G17920	58.3	Yes	No
ACO3	AT2G05710	AT5G49910	33.1	Prey not detected in mito-complexomes	No
CSY4	AT2G44350	AT1G24180	6.5	Yes	11.5 (rank 15)
CSY4	AT2G44350	AT5G14040	5.1	Yes	90 (rank 122)
CSY4	AT2G44350	AT5G49910	16.2	Prey not detected in mito-complexomes	No
FUM1	AT2G47510	AT1G24180	8.6	No	No coexpression data for the bait in ATTED-II
FUM1	AT2G47510	AT4G29840	4.5	Prey not detected in mito-complexomes	No coexpression data for the bait in ATTED-II
FUM1	AT2G47510	AT5G49910	15.0	Prey not detected in mito-complexomes	No coexpression data for the bait in ATTED-II
ICDH	AT5G14590	AT5G49910	22.0	Prey not detected in mito-complexomes	No
IDH1	AT4G35260	AT1G14810	7.2	Yes	No
IDH1	AT4G35260	AT1G48920	85.7	Prey not detected in mito-complexomes	No
IDH1	AT4G35260	AT1G52760	48.1	Yes	174.8 (rank 303)
IDH1	AT4G35260	AT1G55890	10.3	Yes	No
IDH1	AT4G35260	AT2G05990	6.8	No	No
IDH1	AT4G35260	AT2G15620	4.3	Prey not detected in mito-complexomes	No
IDH1	AT4G35260	AT2G33150	5.1	Yes	No
IDH1	AT4G35260	AT2G43750	9.6	Yes	No
IDH1	AT4G35260	AT3G13160	10.3	Yes	No
IDH1	AT4G35260	AT3G13860	5.9	No	No
IDH1	AT4G35260	AT3G15660	7,044.8	Yes	No
IDH1	AT4G35260	AT3G22200	6.8	Yes	No
IDH1	AT4G35260	AT3G47520	10.4	Yes	215.2 (rank 362)
IDH1	AT4G35260	AT3G62530	101.8	Yes	No
IDH1	AT4G35260	AT4G02930	4.3	Yes	No
IDH1	AT4G35260	AT4G24280	11.9	No	No
IDH1	AT4G35260	AT5G19550	4.7	Yes	19.80 (rank 42)
IDH1	AT4G35260	AT5G22650	7.7	Prey not detected in mito-complexomes	No
IDH2	AT2G17130	AT5G14040	8.9	Yes	No
IDH2	AT2G17130	AT5G49910	21.5	Prey not detected in mito-complexomes	No
IDH5	AT5G03290	AT5G49910	16.5	Prey not detected in mito-complexomes	No
IDH6	AT3G09810	AT1G24180	8.9	Bait not detected in mito-complexomes	21.2 (rank 25)
IDH6	AT3G09810	AT3G06050	4.3	Bait not detected in mito-complexomes	319.8 (rank 345)
IDH6	AT3G09810	AT3G09440	5.4	Bait not detected in mito-complexomes	No
IDH6	AT3G09810	AT3G23990	4.5	Bait not detected in mito-complexomes	No
IDH6	AT3G09810	AT4G29840	14.7	Bait not detected in mito-complexomes	No
IDH6	AT3G09810	AT5G12040	5.8	Bait not detected in mito-complexomes	No
IDH6	AT3G09810	AT5G14040	4.7	Bait not detected in mito-complexomes	96.5 (rank 104)
IDH6	AT3G09810	AT5G49910	20.3	Bait not detected in mito-complexomes	No

(*Table continues on following page.*)

Table I. (*Continued from previous page.*)

Bait	Bait AGI Code	Prey[a]	FC-A	Predicted Interaction in Complexome Map[b]	Coexpression (ATTED-II) and Mutual Rank and Occurrence in the First 500 Neighbors[c]
LPD1	AT1G48030	AT1G24180	8.2	No	No
LPD1	AT1G48030	AT3G52200	14.7	Yes	No
LPD2	AT3G17240	AT1G22840	4.4	No	155.1 (rank 155.1)
LPD2	AT3G17240	AT5G03630	7.9	Prey not detected in mito-complexomes	42.6 (rank 86)
LPD2	AT3G17240	AT5G12040	1,929.6	Prey not detected in mito-complexomes	No
MDH2	AT3G15020	AT5G12040	10.9	Prey not detected in mito-complexomes	101.2 (rank 110)
MDH2	AT3G15020	AT5G49910	4.2	Prey not detected in mito-complexomes	No
ME1	AT2G13560	AT5G49910	8.9	Prey not detected in mito-complexomes	No
ODC2-1	AT4G26910	AT1G54220	6.3	No	No
ODC2-1	AT4G26910	AT3G52200	6.7	No	45.4 (rank 66)
ODC2-1	AT4G26910	AT5G12040	4.9	Prey not detected in mito-complexomes	No
ODC2-1	AT4G26910	AT5G49910	590	Prey not detected in mito-complexomes	No
ODC2-2	AT5G55070	AT3G09440	13.4	No	77.3 (rank 61)
ODC2-2	AT5G55070	AT3G13860	5.9	No	No
ODC2-2	AT5G55070	AT3G23990	7.6	No	375.7 (rank 349)
ODC2-2	AT5G55070	AT5G09590	4.1	No	114.9 (rank 99)
ODC2-2	AT5G55070	AT5G12040	8.2	Prey not detected in mito-complexomes	219.2 (rank 199)
ODC2-2	AT5G55070	AT5G14040	10.1	Yes	15.9 (rank 13)
ODC2-2	AT5G55070	AT5G49910	16.6	Prey not detected in mito-complexomes	No
PDC1A-1	AT1G59900	AT1G24180	16.2	Yes	No
PDC1A-1	AT1G59900	AT3G52200	10.4	Yes	No
PDC1B	AT5G50850	AT4G29840	112.8	Prey not detected in mito-complexomes	No
PDC1B	AT5G50850	AT5G49910	6.7	Prey not detected in mito-complexomes	No
PDC2-1	AT1G54220	AT1G24180	10.6	Yes	No
PDC2-1	AT1G54220	AT3G52200	16.7	Yes	No
PDC2-1	AT1G54220	AT5G12040	24.9	Prey not detected in mito-complexomes	152.9 (rank 57)
PDC2-2	AT3G13930	AT1G24180	16.7	Yes	70.8 (rank 75)
PDC2-2	AT3G13930	AT3G52200	27.7	Yes	25.9 (rank 28)
SCOALA-1	AT5G08300	AT3G13860	7.3	No	No
SCOALA-1	AT5G08300	AT5G49910	71.5	Prey not detected in mito-complexomes	No
SCOALA-2	AT5G23250	AT3G13860	8.7	No	252.4 (rank 337)
SCOALA-2	AT5G23250	AT4G24280	8.3	No	No
SDH1-1	AT5G66760	AT2G33210	7.0	No	No
SDH1-1	AT5G66760	AT3G13860	10.8	No	No
SDH1-1	AT5G66760	AT3G23990	23.8	No	No
SDH1-1	AT5G66760	AT4G29840	10.3	Prey not detected in mito-complexomes	No
SDH1-1	AT5G66760	AT5G12040	9.5	Prey not detected in mito-complexomes	No
SDH2-1	AT3G27380	AT3G23990	5.2	No	No
SDH2-1	AT3G27380	AT5G37510	4.7	No	242.3 (rank 248)
SDH2-1	AT3G27380	AT5G49910	36.9	Prey not detected in mito-complexomes	No
SDH2-2	AT5G40650	AT3G13860	4.5	No	No

(*Table continues on following page.*)

Table I. (*Continued from previous page.*)

Bait	Bait AGI Code	Prey[a]	FC-A	Predicted Interaction in Complexome Map[b]	Coexpression (ATTED-II) and Mutual Rank and Occurrence in the First 500 Neighbors[c]
SDH2-2	AT5G40650	AT3G23990	6.6	No	No
SDH2-2	AT5G40650	AT4G37910	4.4	Yes	No
SDH2-2	AT5G40650	AT5G09590	4.7	Yes	No
SDH2-2	AT5G40650	AT5G49910	16.6	Prey not detected in mito-complexomes	No
SDH2-3	AT5G65165	AT3G13860	18.6	Bait not detected in mito-complexomes	No coexpression data for the bait in ATTED-II
SDH2-3	AT5G65165	AT3G23990	11.3	Bait not detected in mito-complexomes	No coexpression data for the bait in ATTED-II
SDH2-3	AT5G65165	AT5G12040	123.3	Bait not detected in mito-complexomes	No coexpression data for the bait in ATTED-II
SDH4	AT2G46505	AT1G24180	8.3	Yes	309.9 (rank 236)
SDH4	AT2G46505	AT3G23990	5.6	No	No
SDH4	AT2G46505	AT3G62530	86.3	Yes	No
SDH4	AT2G46505	AT5G12040	182.6	Prey not detected in mito-complexomes	477.1 (rank 368)
SDH4	AT2G46505	AT5G13450	13.6	No	23.1 (rank 9)
SDH5	AT1G47420	AT1G22840	10.9	No	275.2 (rank 235)
SDH5	AT1G47420	AT1G24180	4.5	No	190.4 (rank 159)
SDH5	AT1G47420	AT2G15620	35.8	Prey not detected in mito-complexomes	No
SDH5	AT1G47420	AT3G55440	4.7	No	22.5 (rank 13)
SDH5	AT1G47420	AT4G29840	4.1	Prey not detected in mito-complexomes	No
SDH5	AT1G47420	AT5G12040	79.1	Prey not detected in mito-complexomes	No
SDH5	AT1G47420	AT5G49910	10.3	Prey not detected in mito-complexomes	No
SDH6	AT1G08480	AT1G22840	17.4	No	51.6 (rank 79)
SDH6	AT1G08480	AT2G05990	5.0	Yes	No
SDH6	AT1G08480	AT2G15620	5.8	Prey not detected in mito-complexomes	No
SDH6	AT1G08480	AT3G52200	4.2	Yes	No
SDH6	AT1G08480	AT4G29840	8.9	Prey not detected in mito-complexomes	No
SDH6	AT1G08480	AT5G12040	23.2	Prey not detected in mito-complexomes	No
SDH6	AT1G08480	AT5G13420	5.0	No	No
SDH6	AT1G08480	ATMG01190	16.3	No	No
SDH7A	AT3G47833	AT2G05990	6.0	Yes	No
SDH7A	AT3G47833	AT4G29840	8.2	Prey not detected in mito-complexomes	No
SDH7A	AT3G47833	AT5G12040	6.1	Prey not detected in mito-complexomes	89.4 (rank 104)
SDH7A	AT3G47833	AT5G13420	11.6	No	No
SDH7A	AT3G47833	AT5G14040	4.3	Yes	No
SDH7A	AT3G47833	AT5G49910	4.3	Prey not detected in mito-complexomes	No
SDH7B	AT5G62575	AT1G22840	102.9	No	367.4 (rank 375)
SDH7B	AT5G62575	AT3G15660	6.2	No	No
SDH7B	AT5G62575	AT4G29840	7.2	Prey not detected in mito-complexomes	No
SDH7B	AT5G62575	AT5G12040	121.7	Prey not detected in mito-complexomes	No
SDH7B	AT5G62575	AT5G13420	16.8	No	No
SDH7B	AT5G62575	AT5G49910	52.4	Prey not detected in mito-complexomes	No
SDH8	AT2G46390	AT2G05990	6.8	Bait not detected in mito-complexomes	No

(*Table continues on following page.*)

Table I. (*Continued from previous page.*)

Bait	Bait AGI Code	Prey[a]	FC-A	Predicted Interaction in Complexome Map[b]	Coexpression (ATTED-II) and Mutual Rank and Occurrence in the First 500 Neighbors[c]
SDH8	AT2G46390	AT3G52200	8.5	Bait not detected in mito-complexomes	No
SDH8	AT2G46390	AT5G12040	685.6	Bait not detected in mito-complexomes	No
SDH8	AT2G46390	AT5G13420	17.5	Bait not detected in mito-complexomes	No

[a]All of the preys are sublocated in mitochondria. All of the positive interactions are the protein pairs, for which the scores were in the top 10%, corresponding to FC-A values of at least 4. [b]Mito-complexomes are the mitochondrial complexomes (Senkler et al., 2017). [c]The coexpression analysis was surveyed by two databases, ATTED-II (Obayashi et al., 2018), which contains Arabidopsis coexpression data gathered from a number of different transcriptomics data sets.

using gas chromatography-mass spectrometry (GC-MS) analysis (Fig. 4A; Supplemental Table S5). In the *amidase* mutant, several TCA cycle intermediates were decreased significantly (here and hereafter, unless stated otherwise, $P < 0.05$), including malic acid, fumaric acid, aconitic acid, and isocitric acid. Several amino acid contents also were decreased significantly, such as Phe, Ser, β-Ala, Gly, and Glu, while the content of Trp was increased. Additionally, Glc, Fru, and altrose contents were decreased significantly more than 4-fold. The contents of Suc and Fuc also were decreased significantly. Several other metabolites also were decreased significantly, such as dehydroascorbic acid, mannitol, putrescine, 3-deoxy-glucosone, and gluconic acid, while lactic acid was increased significantly. In the knockdown mutant of *GRXS15*, several TCA cycle intermediates were increased significantly, including malic acid, fumaric acid, citric acid, and

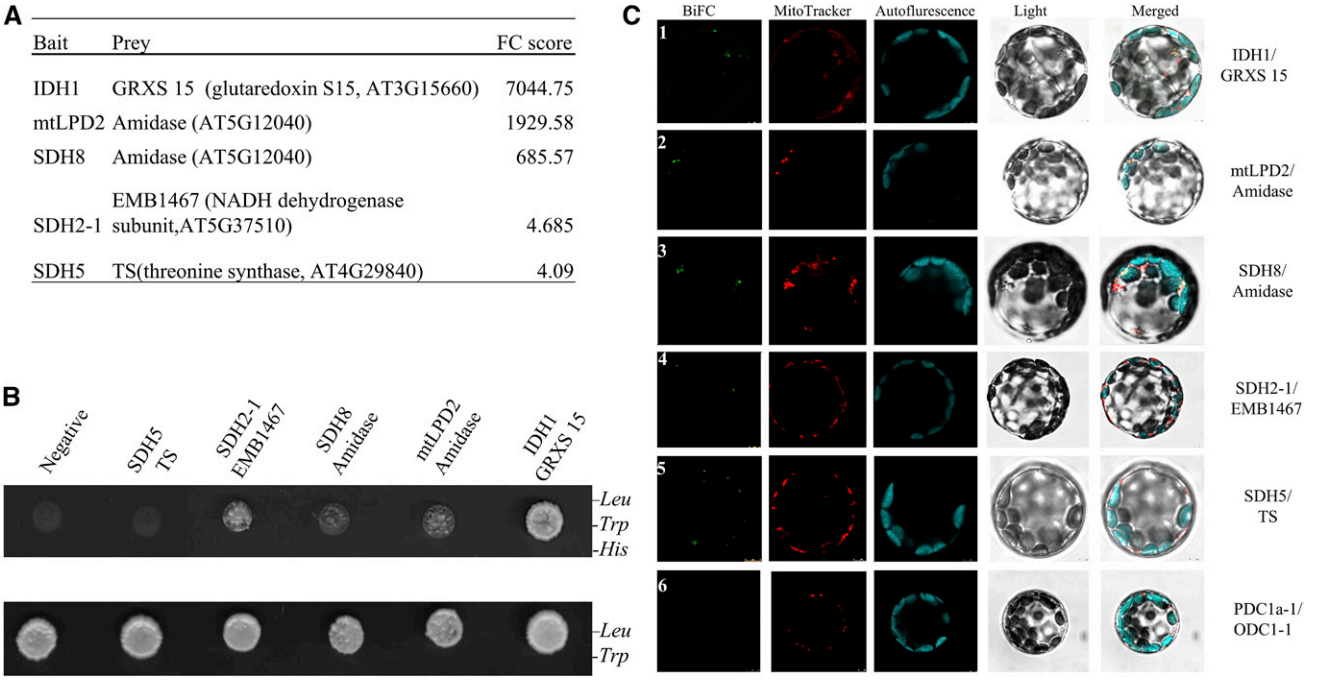

Figure 3. Confirmation of selected protein-protein interactions. A, List of the three high-FC-scoring protein interactions and the two low-scoring interactions that were further tested by Y2H and BiFC. B, Y2H assay to confirm the three high-FC-scoring protein interactions and the two low-scoring interactions. PDC1a-1/ODC1-1 was used as the negative control. The interaction was performed in synthetic dextrose medium with 10 mM 3-aminotriazole and without Leu, Trp, and His. C, The three high-FC-scoring protein interactions and the two low-scoring interactions were tested further by BiFC with transient expression of tagged proteins in Arabidopsis mesophyll protoplasts. Images from left to right show the BiFC signal, fluorescence from MitoTracker Orange staining, autofluorescence, bright-field images, and merged images. Numbered rows are as follows: 1, IDH1-SCYCE/GRXS15-VYNE; 2, mtLPD2-SCYCE/Amidase-VYNE; 3, SDH8-SCYCE/Amidase-VYNE; 4, SDH2-1-SCYCE/EMB1467-VYNE; 5, SDH5-SCYCE/TS-VYNE; 6, PDC1a-1-SCYCE/ODC1-1-VYNE, shown as a representative negative control, which was not detected by affinity purification.

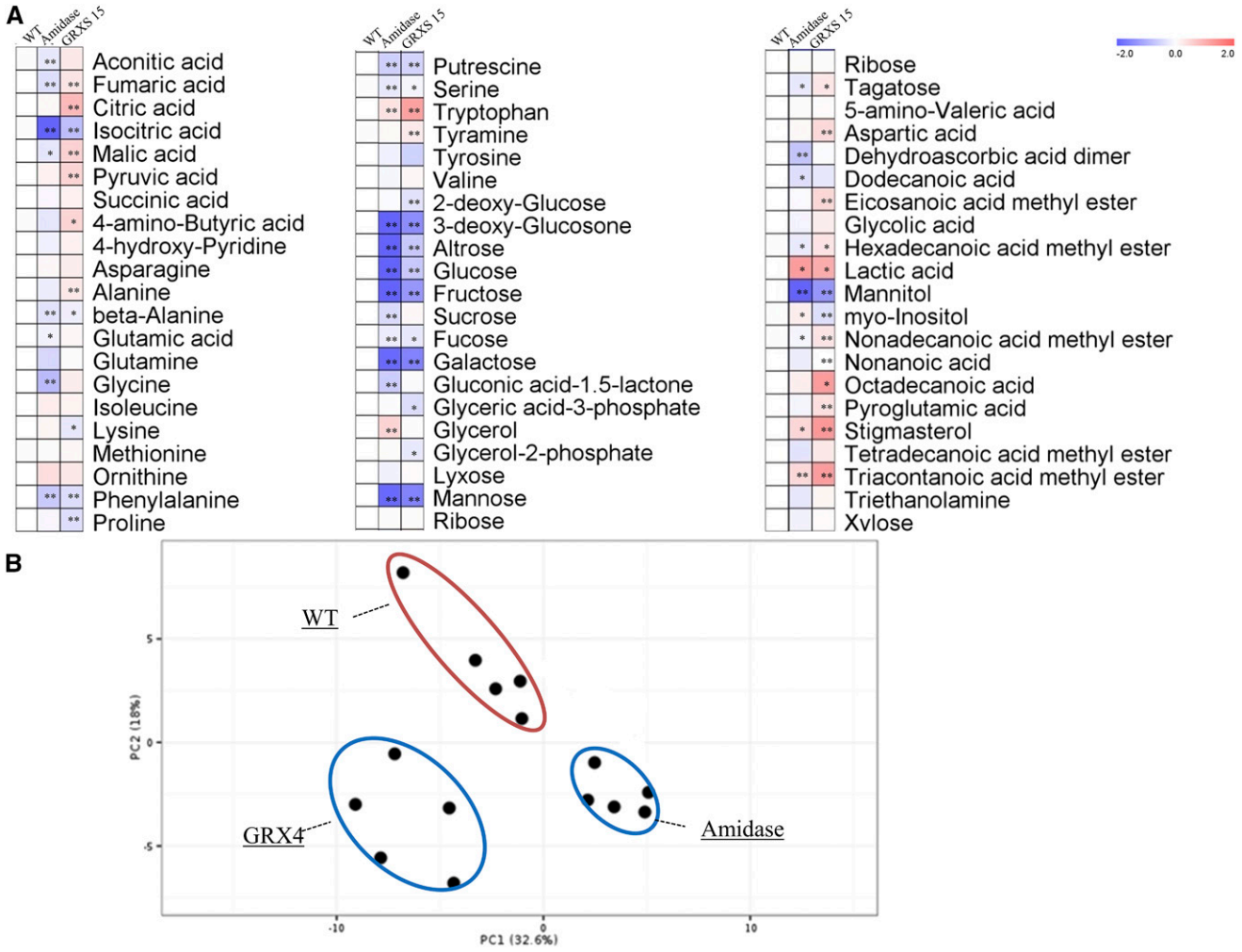

Figure 4. Metabolic content was analyzed using GC-MS. A, Two mutants (*amidase* and *GRX4*), as well as the wild type (WT), were sown on soil and grown for 35 d in short-day conditions (8 h of light/16 h of dark). Metabolic content was analyzed using GC-MS ($n = 5$). Log^2 values of the relative metabolic content are presented. Significant differences compared with the wild type following Student's *t* test are denoted by asterisks (*, $P < 0.05$ and **, $P < 0.01$). B, PCA of the metabolite data.

pyruvic acid, while the content of isocitric acid was decreased. GRXS15 plays an important role in iron-sulfur protein maturation (Moseler et al., 2015) and also affects aconitase activity, lipoic acid-dependent enzymes, and the abundance of isocitrate dehydratase in mitochondria (Ströher et al., 2016). The partial removal of GRXS15 from mitochondria slowed whole-plant growth and respiration (Ströher et al., 2016), decreased the contents of Phe, Lys, Ser, β-Ala, and Pro, and increased the contents of Trp, Ala, Asp, pyro-Glu, tyramine, and butyric acid. Several sugar contents were decreased, including Glc, 2-deoxy-Glc, Fuc, Fru, and altrose. The contents of lactic acid, stigmasterol, nonadecanoic acid, and triacontanoic acid were increased, while glyceric acid-3-phosphate, putrescine, glycerol-2-phosphate, 3-deoxy-glucosone, and mannitol were decreased (Fig. 4A; Supplemental Table S5). Principal component analysis (PCA) demonstrated a separation between the wild type and the two mutant lines (Fig. 4B).

The Relative TCA Flux of Selected Mutants

Given the alteration of several primary metabolites in the mutants, we directly evaluated the respiratory rates of these mutants. We evaluated $^{14}CO_2$ emission using positionally labeled [^{14}C]Glc in order to assess flux through the major pathways of carbohydrate oxidation (Nunes-Nesi et al., 2005). CO_2 is released from the C1 position of Glc by enzymes that are not associated with mitochondrial respiration, unlike CO_2 emission from the C3:4 positions of Glc, which evolved exclusively via reactions associated with the TCA cycle. The ratio of $^{14}CO_2$ emissions from the C1 to C3:4 positions of Glc thus provides an indication of the relative rate

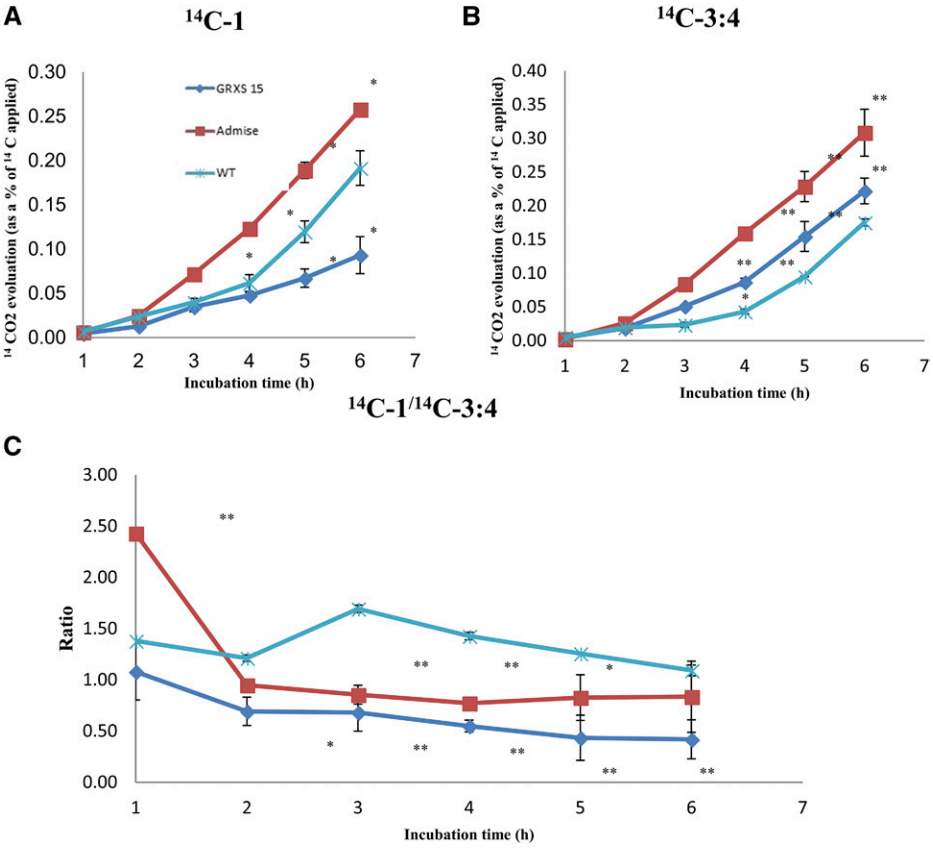

Figure 5. $^{14}CO_2$ emission in the *GRXS15* and *amidase* mutants and the wild type (WT). Emission of $^{14}CO_2$ from the C1 and C3:4 positions of Glc in leaf discs of mutant and wild-type leaves is shown after 35 d of growth under short-day conditions. A, Evolution of $^{14}CO_2$ following incubation in C1-labeled Glc. B, Evolution of $^{14}CO_2$ following incubation in C3:4-labeled Glc. C, Ratio of $^{14}CO_2$ emission from C1 to C3:4 positions, indicating the relative activities of glycolysis and the TCA cycle. Values are means ± SD of determinations on three to four independent samples. Significant differences compared with the wild type following Student's *t* test are denoted by asterisks (*, $P < 0.05$ and **, $P < 0.01$).

of glycolysis and the TCA cycle, with smaller ratios indicating a relative increase in the flux through the TCA cycle (Avin-Wittenberg et al., 2015). Although the level of C1 emission was higher in the *amidase* mutant and lower in the *GRX* mutant than in the wild type, the level of C3:4 emission was increased in both mutants (Fig. 5, A and B). Thus, when considering the C1-C3:4 CO_2 emission ratio, the ratio for the wild type is higher than that of the two mutants (from 1 to 5 h), suggesting that a higher proportion of carbohydrate oxidation is performed by the TCA cycle in both mutants (Fig. 5C) and, thus, providing an indirect functional confirmation of cooperativity of the proteins in question.

DISCUSSION

In a previous study, we characterized the protein-protein interactions within the mitochondrial TCA cycle and revealed a total of 158 interactions between sequential and nonsequential enzymes of the TCA cycle (Zhang et al., 2017a). A similar study, albeit one based solely on bacterial two-hybrid assays, suggests that similar levels of interactions were present in *Bacillus subtilis* (Meyer et al., 2011). These studies provide evidence suggesting that the degree of interaction between the TCA cycle enzymes is greater than that suggested by classical biochemical studies based on the copurification of enzymes, which Paul Srere first used to define his concept of the metabolon (Srere, 1985). Individually, these data are not sufficient to demonstrate metabolite channeling, and for this reason, we additionally performed isotope dilution experiments in an earlier study, in which labeled precursors and unlabeled intermediates were supplied to the pharmacologically linearized TCA cycle (Zhang et al., 2017a). These experiments suggested that channeling existed in the well-characterized malate dehydrogenase, citrate synthase, and aconitase complex (Vélot et al., 1997; Wu and Minteer, 2015) and also indicated the possibility of channeling between fumarate and malate dehydrogenase and between aconitase and isocitrate dehydrogenase. Intriguingly, despite following a much more focused approach, the early biochemical studies of Srere, Sumegi, and coworkers revealed not only protein-protein interactions between the TCA cycle enzymes themselves but also with several other matrix proteins, such as enzymes of fatty acid oxidation (Sumegi and Srere, 1984a), complex I (NADH dehydrogenase; Sumegi and Srere, 1984b), and even the Asp-malate shuttle and citrate transporter proteins of the mitochondrial carrier family (Beeckmans and Kanarek, 1981; Grigorenko et al., 1990).

In this study using AP-MS (Zhang et al., 2017a), we identified interactions between TCA cycle enzymes and matrix proteins, including interactions with the homologs of fatty acids and NADH dehydrogenase reported in the studies mentioned above and

an interaction with a putative phosphate transporter of the mitochondrial carrier family, although not with homologs of the citrate or Asp-malate transporters described above. As well as being highly important molecules within plants, amino acids additionally serve as precursors of a wide variety of natural plant products that play crucial roles in plant growth, development, and stress tolerance. TCA cycle intermediates provide the carbon skeletons to support the biosynthesis of the majority of amino acids (Nunes-Nesi et al., 2013; Galili et al., 2016). A large portion of the matrix enzymes serve anapleurotic roles in supplying the amino acid biosynthetic enzymes with carbon skeletons.

Amino acid synthesis in the light is strongly dependent on the remobilization of carbon skeletons from acetyl-CoA and citrate (Gauthier et al., 2010). The maintenance of these biosynthetic fluxes may be aided, in part, by the protein interaction between aconitase (ACO2) and Met synthase (AT5G17920) and between IDH1 and acetyl-CoA C-acyltransferase (AT2G33150), Asp aminotransferase (AT5G19550), 4-aminobutyrate transaminase (AT3G22200), Cys synthase (AT2G43750), semialdehyde dehydrogenase (AT1G14810), and nitrite reductase1 (AT2G15620; Supplemental Tables S3 and S4). Given that the IDH1 sequence contains a regulatory domain (Lemaitre et al., 2007), it is possible that these interactions with amino acid-related proteins could play an important role in regulating amino acid content. In keeping with this hypothesis, the levels of several metabolite contents were altered significantly in the IDH1 mutant, with prominent changes for isocitrate, Asp, Asn, Cys, Ser, and Thr (Lemaitre et al., 2007). These findings provide support for a potential functional advantage of these protein interactions. However, future studies using the more elegant approaches of mutation and/or truncation of protein-protein interaction domains while preserving enzymatic activity will be required in order to confirm this hypothesis and provide a more rigorous mechanistic understanding of the function of these interactions. Similarly, the interactions between mitochondrial lipoamide dehydrogenase2 (mtlpd2), mitochondrial pyruvate dehydrogenase complex 2-1 (PDC2-1), and amidase (AT5G12040) are consistent with the changes in the levels of Asn and oxoglutarate in the *amidase* mutant (Zhang and Marsolais, 2014). Similarly, Thr synthase (AT4G29840) interacted with PDC1B, IDH6, several subunits of SDH, and fumarase (FUM1), indicating that the TCA cycle may directly fuel Thr synthesis.

We believe that, as mentioned above for the IDH interaction, the study of the amidase interactions and, indeed, all other interactions uncovered in our protein interaction network provides important leads that, when followed up by more detailed genetic and biochemical analyses, will likely yield considerably more information on the molecular basis underlying these metabolic linkages. Furthermore, they also could provide support that amino acids are efficiently catabolized into the TCA cycle to generate the cellular energy required for plant growth, particularly in response to stresses that create energy deprivation. However, it is important to note that, while these studies provide far greater surety than methods based on coexpression alone (Wang et al., 2012), further experimental evidence will ultimately be required in order to fully comprehend their reliability and functionality, and these lists should be used currently as a guide only.

The above caveat aside, the occurrence of many of the interactions that were detected here does have a clear precedence in the literature. For example, ATP synthase interacted with succinate dehydrogenase (Ardehali et al., 2004) and is proposed to organize the supercomplex with the TCA cycle metabolon in the inner membrane of mitochondria (Seelert and Dencher, 2011). The protein supercomplex structure of the mETC complexes has been postulated to support a protein-protein interaction-mediated substrate channel (Letts et al., 2016), although this postulate is very much debated (Lenaz et al., 2016; Milenkovic et al., 2017). In our data set, several subunits of succinate dehydrogenase were found to interact with other complexes of the mETC. For example, SDH5/SDH6/SDH7B interacted with cytochrome C-1 (AT1G22840), SDH6 interacted with ATPase subunit 1 (ATMG01190), SDH4 interacted with the δ-subunit of ATP synthase (AT5G13450), and SDH2-1 interacted with embryo-defective1467 (EMB1467 [AT5G37510]; Fig. 2A; Supplemental Table S3). It is important to note here that cyt-C1 and SDH5 are localized at opposite sides of the inner mitochondrial membrane; hence, their interaction must occur indirectly via a multilateral interaction and bridging via other proteins, most likely the other SDH subunits. However, further confirmatory binary interaction analyses will be required in order to validate this hypothesis.

When our results are compared with those obtained following digestion (and subsequent MS analyses) of electrophoretically separated supercomplexes (Senkler et al., 2017), a considerable degree of overlap is apparent (Table I). Although some of the partners of our interactions could not be detected in the complexome map, and given that the results of the two studies are not directly comparable, the overlap does provide circumstantial support for the fidelity of many of the interactions we report (Supplemental Fig. S3). As an additional cross check, with the aim of comparing the results presented here with our previously published data, we checked whether our set of validated interactions could have been obtained simply by chance alone through random resampling of the initial set of 257 interactions. None of the 1 million random resamplings yielded a combination equal to our list of validated interactions, providing further support to the non-random nature of the interactions reported here.

Several steps of the TCA cycle are subject to redox regulation by the thioredoxin system (Daloso et al., 2015). The importance of the interaction of redox and the TCA cycle is further supported in this study by the direct interactions of IDH6 with peroxiredoxin IIF

(AT3G06050) and mtlpd2 with pyridine nucleotide-disulfide oxidoreductase (AT5G03630), although members of the thioredoxin family itself did not copurify with any TCA cycle enzymes.

In addition to the interactions described above, the interaction network we report here also revealed other less well-understood and even entirely unreported connections. Among the former was the observation, as reported previously in mammalian mitochondria (James et al., 2002), that the heat shock protein chaperones HSP60 and HSP70 interacted with aconitase and the oxoglutarate dehydrogenase complex (ODC), respectively. Such interactions have been proposed either to aid in correct protein folding or to stabilize enzyme functions under conditions of stress. Interactions that are, to our knowledge, previously unreported include those related to lipid metabolism and signal transduction (Supplemental Table S6), including two lipid-related proteins (mosaic death1 and esterase) that interacted with IDH and SDH and four signal transduction-related proteins interacting with IDH, ODC, SDH, and PDC (Supplemental Table S6). Furthermore, the six stress-related proteins, including tetratricopeptide repeat-like superfamily proteins and ARM repeat superfamily proteins, also interacted with TCA cycle enzymes. All of the above-mentioned interactions are easy to rationalize from a functional perspective. However, they clearly need extensive follow-up studies in order to validate their roles in vivo.

Unlike binary protein-protein interaction methods that focus on detecting direct physical interactions, AP-MS is designed to identify complex interactions that include both direct physical interactions (between proteins that share a common binding interface) and indirect cocomplex associations (between proteins that do not interact physically with each other but belong to common complexes). As mentioned above, five interacting pairs were selected for further study on the basis of their FC scores, and both Y2H assays and complementary BiFC assays support the interaction of these pairs. It is important to note that these approaches are based on different principles (affinity purification and split molecular complementation) and were performed in widely differing physiological conditions (Arabidopsis heterotrophic cell suspension culture, yeast cells, and mesophyll protoplasts). As such, it can be anticipated that this interaction network provides strongly positive protein interaction information for many interactions, although empirical validation will ultimately be required for each of the remaining 120 extra-pathway interactions reported here.

As a first step to further analyze the function of the extra-pathway interactions of TCA cycle enzymes, which we confirmed via alternate methods, metabolite content and ^{14}C-labeled flux redistribution were determined in *GRXS15* and *amidase* mutants. Consistent with the interactions of GRX and amidase with the IDH complex enzymes (Fig. 3A; Supplemental Table S3), the isocitrate content was altered significantly in both mutants, as was the relative flux through the TCA cycle (Figs. 4 and 5). Additionally, the contents of malate, fumarate, and Glu differed between the wild type and the *amidase* mutant. This observation may reflect the fact that the amidase protein interacted physically with MDH, SDH, and ODC (Fig. 2A). As the function of amidase is related to amino acid metabolism, it is interesting that the changes of several amino acids have been published for the mutant of its interactor IDH (Lemaitre et al., 2007). As the CO_2 emissions from the C3:4 positions of Glc evolved via reactions associated with the TCA cycle, the levels of C3:4 emissions in both lines were increased, indicating increased TCA flux. Additionally, the relative increase in TCA cycle flux also is supported by the smaller ratio of CO_2 emission from the relative rate of glycolysis and the TCA cycle. Both the metabolite and flux data support the potential function of the interactions of GRX and amidase with the TCA cycle enzymes, although this evidence is circumstantial.

The advent of AP-MS has resulted in a dramatic increase in our understanding of functional protein-protein interactions, allowing many important advances in diverse model organisms spanning the tree of life (Morris et al., 2014). Our previous study of the interactions between plant TCA cycle enzymes revealed the assembly of higher order, noncovalently linked metabolons, which channel metabolites through sequential steps of the TCA cycle (Zhang et al., 2017a). However, interactions between noncatalytic subunits or catalytic subunits of nonsequential reactions may additionally serve to constrain the enzymes within close proximity to one another (Supplemental Fig. S2A). In addition, the 125 novel interactions between TCA cycle enzymes and the 37 mitochondrial protein preys described here allow us greater insight concerning the spatial aspects of the role of the TCA cycle in amino acid metabolism, mETC/ATP synthesis, redox, and stress. These data provide an important basis toward a better understanding of the mechanisms underlying the functional interaction of the TCA cycle and a plethora of other metabolic pathways and processes. On the other hand, they reenforce the idea that the TCA cycle is highly important in providing substrates for nitrogen and amino acid metabolism and mETC/ATP synthesis, and they pinpoint new potential regulatory roles in the processes of lipid metabolism, signaling, and response to stress.

Beyond the specific details presented here, we believe that this study additionally demonstrates the power of carrying out AP-MS, alongside the appropriate validation techniques, at the entire pathway level as a means of identifying functional interactions between both intimately and mildly interlinked processes. Given the scale of interacting partners identified here, it is clear that this technique currently cannot validate each and every interaction; however, it provides compelling hypotheses that can be tested via further rounds of experimentation.

MATERIALS AND METHODS

cDNA Cloning and Vector Construction

The mitochondrially localized Arabidopsis (*Arabidopsis thaliana*) proteins involved in the TCA cycle were selected by reference to the literature (Nunes-Nesi et al., 2013); thus, the list totaled 38 proteins (Supplemental Table S7). Full-length coding sequences of these proteins were cloned from a cDNA pool generated from 2-week-old Arabidopsis Columbia-0 (Col-0) ecotype plants by PCR-based Gateway BP cloning using the pDONR207 donor vector (Thermo Fisher Scientific). The gene-specific primers used did not include a stop codon to ensure C-terminal fusion of tags (Supplemental Table S8). Expression vectors for AP-MS, BiFC, and Y2H were constructed using the Gateway LR reaction with pK7FWG2 (Karimi et al., 2002), pDuvyNE and pDuScyCE (Zhang et al., 2017a), and pGADCg and pGBKCg, respectively (Supplemental Table S9).

Plant Growth Conditions

Arabidopsis genotypes Col-0 (the wild type), *GRXS15* (Salk_112767 [Col-0 background]; Ströher et al., 2016), and *amidase* (Sail_608_A02 [Col-0 background]; Zhang and Marsolais, 2014) mutants were used in this study. The seeds were plated on Murashige and Skoog medium supplemented with 1% (w/v) Suc for 10 d, then the seedlings were transferred to soil under an 8-h-light (22°C)/16-h-dark (18°C) period in a growth chamber at a light intensity of 120 to 150 µmol m^{-2} s^{-1}. The prebolting mature rosette leaves of 35-d-old plants were harvested for metabolite measurements and estimation of respiratory flux at the beginning of the day.

AP-MS

AP-MS was conducted by expressing target proteins fused with a C-terminal GFP tag in the PSB-D Arabidopsis cell culture line using a published protocol (Van Leene et al., 2011). Tandem GFP fused with an N-terminal mitochondria-targeting peptide was used as a negative control. PSB-D cells (Arabidopsis Biological Resource Center) were cultured in the dark at 25°C with shaking at 120 rpm. The cell line was cultured on Murashige and Skoog basal salts with minimal organics medium (Sigma-Aldrich) supplemented with 50 µg L^{-1} kinetin, 0.5 mg L^{-1} 1-naphthaleneacetic acid, and 3% (w/v) Suc.

Cells were subcultured every week at a 1:10 culture-to-fresh medium ratio. *Agrobacterium tumefaciens* strain GV3101 pMP90 transformed with an expression vector was grown on a plate for 2 d and then scratched and resuspended into Murashige and Skoog basal salts with minimal organics medium to gain an OD_{600} of 1. A 3-mL aliquot of 2-d-old PSB-D cell culture was mixed with 200 µL of *A. tumefaciens* suspension and 6 µL of 100 mM acetosyringone and cocultivated for 72 h. Transformed cells were selected in a medium containing 25 µg L^{-1} kanamycin, 500 µg L^{-1} carbenicillin, and 500 µg L^{-1} vancomycin for three rounds of a 1-week subculture followed by those with medium containing only kanamycin for two rounds (Van Leene et al., 2011). Expression and localization of the tagged proteins were evaluated by viewing GFP fluorescence using confocal microscopy. The transformed cells were collected by vacuum filtration at 5 d after subculturing and frozen in liquid nitrogen. After grinding into a fine powder using a ball mill (MM301; Retsch), proteins were extracted by mixing 2 g of material with 2 mL of extraction buffer (25 mM Tris-HCl, pH 7.5, 15 mM $MgCl_2$, 5 mM EGTA, 1 mM DTT, and 1 mM PMSF). Following the removal of cell debris by repeated centrifugation at 22,000*g* at 4°C for 5 min, the supernatant was mixed with 25 µL of GFP-Trap_A slurry (ChromoTek) equilibrated with extraction buffer and incubated for 1 h at 4°C with rotation. The beads were collected by centrifugation at 3,000*g* at 4°C for 3 min and washed three times each with extraction buffer containing 0, 250, and 500 mM NaCl.

The proteins remaining on the beads were subsequently subjected to proteomics as in-solution digestion by LysC and trypsin, and the resulting peptides were purified (Wiśniewski et al., 2009). LC-MS/MS analysis was performed on Q Exactive Plus (Thermo Fisher Scientific). Quantitative analysis of MS/MS measurements was performed with the Progenesis IQ software (Nonlinear Dynamics). Proteins were identified from spectra using Mascot (Matrix Science). Mascot search parameters were set as follows: TAIR10 protein annotation; requirement for tryptic ends; one missed cleavage allowed; fixed modification, carbamidomethylation (Cys); variable modification, oxidation (Met); peptide mass tolerance, ±10 ppm; MS/MS tolerance, ±0.6 D; allowed peptide charges of +2 and +3. A decoy database search was used to limit false discovery rates to 1% on the protein level. Peptide identifications below rank 1 or with a Mascot ion score below 25 were excluded. Mascot results were imported into Progenesis QI, quantitative peak area information was extracted, and the results were exported for data plotting and statistical analysis. These intensities were filtered against the experiment control and normalized using the spectral index in the CRAPome Web site (Mellacheruvu et al., 2013). Finally, the possible interactions were scored as FC-A calculated by the SAINT algorithm (Choi et al., 2012; Mellacheruvu et al., 2013; Supplemental Table S1; Supplemental Fig. S1).

Our affinity purification was performed in five different experiments resulting in at least three independent biological replicates, with FC-A values being calculated for each individual replicate. All of the FC-A scores of the detected peptides are presented in Supplemental Table S1. Finally, the interaction pairs with FC score above 4 were selected and analyzed by SUBA4 (Hooper et al., 2017) in order to restrict defined interactors to those proteins that are colocalized to the mitochondria (Supplemental Table S3). The resultant protein-protein interaction network was visualized by Cytoscape (Shannon et al., 2003) using the data shown in Supplemental Table S3.

BiFC

BiFC constructs were expressed in mesophyll protoplasts, which were generated from the leaves of Arabidopsis Col-0 by the Tape-Arabidopsis Sandwich method (Wu et al., 2009). Briefly, the lower epidermal surface of a leaf was removed by peeling with a strip of tape fixed to it. The mesophyll cells remaining on the tape were incubated in 20 mM MES buffer (pH 5.7) containing 1% cellulose (Yakult), 0.25% macerozyme (Yakult), 10 mM $CaCl_2$, 20 mM KCl, 0.1% BSA, and 0.4 M mannitol with gentle agitation for 20 to 60 min until the protoplasts were released into the solution. The protoplasts were washed twice with W5 solution (2 mM MES, pH 5.7, 154 mM NaCl, 125 mM $CaCl_2$, 5 mM KCl, and 5 mM Glc), incubated on ice for 30 min, centrifuged, and resuspended into MMg solution (4 mM MES, pH 5.7, 15 mM $MgCl_2$, and 0.4 M mannitol). Protoplasts were transfected with plasmids on a U-bottom 96-well plate by incubating for 5 min at room temperature in the presence of 20% (w/v) PEG4000. Following two washings with W5 solution, the protoplasts were incubated in the dark at 25°C overnight (Kato and Jones, 2010). The protoplasts were incubated with MitoTracker Orange CMTMRos (Thermo Fisher Scientific) for mitochondrial staining at 37°C for 10 min followed by 26°C for 20 min. Confocal images were taken using a DM6000B/SP5 confocal laser scanning microscope (Leica Microsystems). BiFC and MitoTracker fluorescence were imaged with 488- and 555-nm laser excitation, and emission fluorescence was captured by 500- to 520-nm and 560- to 580-nm band-pass emission filters, respectively.

Y2H Assay

The expression clones for the Y2H assay were transformed into yeast mating strains AH109 and Y187 as described by Roberts et al. (2012). Binary protein interactions were tested by direct mating of a set of baits with a set of preys expressed in opposite yeast mating types (Stellberger et al., 2010). Transformants containing both bait and prey constructs were inoculated on synthetic dextrose plates without Leu, Trp, and His but containing 3-aminotriazole, as described by Stellberger et al. (2010), and colony formation was scored 3 d post inoculation.

Estimation of Fluxes

Estimation of respiratory flux on the basis of $^{14}CO_2$ emission was carried out as described (Kühn et al., 2015). Twenty leaf discs (7 mm in diameter) of plants at the same growth stage after 35 d of short-day conditions were incubated in 5 mL of medium (50 mM MES, pH 6.5, containing 0.3 mM Glc labeled with 6.2 MBq $mmol^{-1}$ ^{14}C at position 1 and positions 3 and 4 [ARC0120A and ARC0211, respectively]; American Radiolabeled Chemicals) in closed flasks. Evolved $^{14}CO_2$ was trapped in 500 mL of 10% (w/v) KOH inserted in the flask, with the trap being replaced by a fresh one every 1 h. The entire KOH solution in the trap was mixed with 4 mL of scintillation cocktail (Rotizint Eco Plus; Roth), and radioactivity was determined using a liquid scintillation counter (LS6500; Beckman Coulter).

Metabolite Measurement

Metabolite profiling of Arabidopsis leaves was carried out by GC-MS (ChromaTOF software, Pegasus driver 1.61; LECO) as described previously

(Lisec et al., 2006). The chromatograms and mass spectra were evaluated using TagFinder software (Luedemann et al., 2012). Metabolite identification was checked manually by the mass spectral and retention index collection of the Golm Metabolome Database (Kopka et al., 2005). Peak heights of the mass fragments were normalized on the basis of the fresh weight of the sample and the added amount of an internal standard (ribitol). Statistical differences between groups were analyzed by Student's *t* test on the raw data. The results were determined to be statistically different at $P < 0.05$. Relative metabolite levels were obtained as the ratio between the lines and the mean value of the respective wild type. PCA was performed using a prewritten R script.

Accession Numbers

Sequence data from this article can be found in the GenBank/EMBL data libraries under accession numbers of AGI code.

Supplemental Data

The following supplemental materials are available.

Supplemental Figure S1. Detailed work process of the affinity purification.

Supplemental Figure S2. Separate graphical representation of the binary protein-protein interaction network of Arabidopsis TCA cycle enzymes.

Supplemental Figure S3. Overlap between the 125 extra-pathway interactions with those retrieved from the complexome map of Arabidopsis mitochondria (Senkler et al., 2017).

Supplemental Table S1. List of all of the interaction FC.

Supplemental Table S2. List of the interactions found in at least three replicates.

Supplemental Table S3. List of the proteins with interaction FC greater than 4-fold.

Supplemental Table S4. List of the 11 groups of prey as classified by MAPMAN.

Supplemental Table S5. Metabolic content as analyzed by GC-MS.

Supplemental Table S6. List of interactions related to lipid metabolism, transporters, and signal transduction.

Supplemental Table S7. List of the proteins tested in this study.

Supplemental Table S8. Primers used in this study.

Supplemental Table S9. Plasmids constructed in this study.

ACKNOWLEDGMENTS

We thank Dr. Geert de Jaeger and Dr. Jelle Van Leene (VIB) for providing the PSB-D cell culture and A. Harvey Millar for providing seeds of GRXS15 (Salk_112767).

Received November 21, 2017; accepted May 14, 2018; published May 23, 2018.

LITERATURE CITED

Araújo WL, Nunes-Nesi A, Nikoloski Z, Sweetlove LJ, Fernie AR (2012) Metabolic control and regulation of the tricarboxylic acid cycle in photosynthetic and heterotrophic plant tissues. Plant Cell Environ **35**: 1–21

Ardehali H, Chen Z, Ko Y, Mejía-Alvarez R, Marbán E (2004) Multiprotein complex containing succinate dehydrogenase confers mitochondrial ATP-sensitive K+ channel activity. Proc Natl Acad Sci USA **101**: 11880–11885

Avin-Wittenberg T, Bajdzienko K, Wittenberg G, Alseekh S, Tohge T, Bock R, Giavalisco P, Fernie AR (2015) Global analysis of the role of autophagy in cellular metabolism and energy homeostasis in *Arabidopsis* seedlings under carbon starvation. Plant Cell **27**: 306–322

Beeckmans S, Kanarek L (1981) Demonstration of physical interactions between consecutive enzymes of the citric acid cycle and of the aspartate-malate shuttle: a study involving fumarase, malate dehydrogenase, citrate synthesis and aspartate aminotransferase. Eur J Biochem **117**: 527–535

Bürckstümmer T, Bennett KL, Preradovic A, Schütze G, Hantschel O, Superti-Furga G, Bauch A (2006) An efficient tandem affinity purification procedure for interaction proteomics in mammalian cells. Nat Methods **3**: 1013–1019

Choi H, Liu G, Mellacheruvu D, Tyers M, Gingras AC, Nesvizhskii AI (2012) Analyzing protein-protein interactions from affinity purification-mass spectrometry data with SAINT. Curr Protoc Bioinformatics **8**: 15

Daloso DM, Müller K, Obata T, Florian A, Tohge T, Bottcher A, Riondet C, Bariat L, Carrari F, Nunes-Nesi A, (2015) Thioredoxin, a master regulator of the tricarboxylic acid cycle in plant mitochondria. Proc Natl Acad Sci USA **112**: E1392–E1400

Galili G, Amir R, Fernie AR (2016) The regulation of essential amino acid synthesis and accumulation in plants. Annu Rev Plant Biol **67**: 153–178

Gauthier PP, Bligny R, Gout E, Mahé A, Nogués S, Hodges M, Tcherkez GG (2010) In folio isotopic tracing demonstrates that nitrogen assimilation into glutamate is mostly independent from current CO2 assimilation in illuminated leaves of *Brassica napus*. New Phytol **185**: 988–999

Gehl C, Waadt R, Kudla J, Mendel RR, Hänsch R (2009) New GATEWAY vectors for high throughput analyses of protein-protein interactions by bimolecular fluorescence complementation. Mol Plant **2**: 1051–1058

Giegé P, Heazlewood JL, Roessner-Tunali U, Millar AH, Fernie AR, Leaver CJ, Sweetlove LJ (2003) Enzymes of glycolysis are functionally associated with the mitochondrion in *Arabidopsis* cells. Plant Cell **15**: 2140–2151

Graham JW, Williams TC, Morgan M, Fernie AR, Ratcliffe RG, Sweetlove LJ (2007) Glycolytic enzymes associate dynamically with mitochondria in response to respiratory demand and support substrate channeling. Plant Cell **19**: 3723–3738

Grigorenko EV, Small WC, Persson LO, Srere PA (1990) Citrate synthase 1 interacts with the citrate transporter of yeast mitochondria. J Mol Recognit **3**: 215–219

Hooper CM, Castleden IR, Tanz SK, Aryamanesh N, Millar AH (2017) SUBA**4**: the interactive data analysis centre for Arabidopsis subcellular protein locations. Nucleic Acids Res **45**: D1064–D1074

James EA, Gygi SP, Adams ML, Pierce RH, Fausto N, Aebersold RH, Nelson SD, Bruschi SA (2002) Mitochondrial aconitase modification, functional inhibition, and evidence for a supramolecular complex of the TCA cycle by the renal toxicant S-(1,1,2,2-tetrafluoroethyl)-L-cysteine. Biochemistry **41**: 6789–6797

Jørgensen K, Rasmussen AV, Morant M, Nielsen AH, Bjarnholt N, Zagrobelny M, Bak S, Møller BL (2005) Metabolon formation and metabolic channeling in the biosynthesis of plant natural products. Curr Opin Plant Biol **8**: 280–291

Karimi M, Inzé D, Depicker A (2002) GATEWAY vectors for Agrobacterium-mediated plant transformation. Trends Plant Sci **7**: 193–195

Kato N, Jones J (2010) The split luciferase complementation assay. Methods Mol Biol **655**: 359–376

Kopka J, Schauer N, Krueger S, Birkemeyer C, Usadel B, Bergmüller E, Dörmann P, Weckwerth W, Gibon Y, Stitt M, (2005) GMD@CSB.DB: the Golm Metabolome Database. Bioinformatics **21**: 1635–1638

Kühn K, Obata T, Feher K, Bock R, Fernie AR, Meyer EH (2015) Complete mitochondrial complex I deficiency induces an up-regulation of respiratory fluxes that is abolished by traces of functional complex I. Plant Physiol **168**: 1537–1549

Laursen T, Borch J, Knudsen C, Bavishi K, Torta F, Martens HJ, Silvestro D, Hatzakis NS, Wenk MR, Dafforn TR, (2016) Characterization of a dynamic metabolon producing the defense compound dhurrin in sorghum. Science **354**: 890–893

Lemaitre T, Urbanczyk-Wochniak E, Flesch V, Bismuth E, Fernie AR, Hodges M (2007) NAD-dependent isocitrate dehydrogenase mutants of Arabidopsis suggest the enzyme is not limiting for nitrogen assimilation. Plant Physiol **144**: 1546–1558

Lenaz G, Tioli G, Falasca AI, Genova ML (2016) Complex I function in mitochondrial supercomplexes. Biochim Biophys Acta **1857**: 991–1000

Letts JA, Fiedorczuk K, Sazanov LA (2016) The architecture of respiratory supercomplexes. Nature **537**: 644–648

Lisec J, Schauer N, Kopka J, Willmitzer L, Fernie AR (2006) Gas chromatography mass spectrometry-based metabolite profiling in plants. Nat Protoc **1**: 387–396

Luedemann A, von Malotky L, Erban A, Kopka J (2012) TagFinder: preprocessing software for the fingerprinting and the profiling of gas chromatography-mass spectrometry based metabolome analyses. Methods Mol Biol**860**: 255–286

Mellacheruvu D, Wright Z, Couzens AL, Lambert JP, St-Denis NA, Li T, Miteva YV, Hauri S, Sardiu ME, Low TY, (2013) The CRAPome: a contaminant repository for affinity purification-mass spectrometry data. Nat Methods **10**: 730–736

Meyer FM, Gerwig J, Hammer E, Herzberg C, Commichau FM, Völker U, Stülke J (2011) Physical interactions between tricarboxylic acid cycle enzymes in *Bacillus subtilis*: evidence for a metabolon. Metab Eng **13**: 18–27

Milenkovic D, Blaza JN, Larsson NG, Hirst J (2017) The enigma of the respiratory chain supercomplex. Cell Metab **25**: 765–776

Morris JH, Knudsen GM, Verschueren E, Johnson JR, Cimermancic P, Greninger AL, Pico AR (2014) Affinity purification-mass spectrometry and network analysis to understand protein-protein interactions. Nat Protoc **9**: 2539–2554

Moseler A, Aller I, Wagner S, Nietzel T, Przybyla-Toscano J, Mühlenhoff U, Lill R, Berndt C, Rouhier N, Schwarzländer M, (2015) The mitochondrial monothiol glutaredoxin S15 is essential for iron-sulfur protein maturation in *Arabidopsis thaliana*. Proc Natl Acad Sci USA **112**: 13735–13740

Nunes-Nesi A, Carrari F, Lytovchenko A, Smith AM, Loureiro ME, Ratcliffe RG, Sweetlove LJ, Fernie AR (2005) Enhanced photosynthetic performance and growth as a consequence of decreasing mitochondrial malate dehydrogenase activity in transgenic tomato plants. Plant Physiol **137**: 611–622

Nunes-Nesi A, Araújo WL, Obata T, Fernie AR (2013) Regulation of the mitochondrial tricarboxylic acid cycle. Curr Opin Plant Biol **16**: 335–343

Obayashi T, Aoki Y, Tadaka S, Kagaya Y, Kinoshita K (2018) ATTED-II in **2018**: a plant coexpression database based on investigation of the statistical property of the mutual rank index. Plant Cell Physiol **59**: e3

Panicot M, Minguet EG, Ferrando A, Alcázar R, Blázquez MA, Carbonell J, Altabella T, Koncz C, Tiburcio AF (2002) A polyamine metabolon involving aminopropyl transferase complexes in *Arabidopsis*. Plant Cell **14**: 2539–2551

Puig O, Caspary F, Rigaut G, Rutz B, Bouveret E, Bragado-Nilsson E, Wilm M, Séraphin B (2001) The tandem affinity purification (TAP) method: a general procedure of protein complex purification. Methods **24**: 218–229

Roberts GG III, Parrish JR, Mangiola BA, Finley RL Jr (2012) High-throughput yeast two-hybrid screening. Methods Mol Biol **812**: 39–61

Seelert H, Dencher NA (2011) ATP synthase superassemblies in animals and plants: two or more are better. Biochim Biophys Acta **1807**: 1185–1197

Senkler J, Senkler M, Eubel H, Hildebrandt T, Lengwenus C, Schertl P, Schwarzländer M, Wagner S, Wittig I, Braun HP (2017) The mitochondrial complexome of *Arabidopsis thaliana*. Plant J **89**: 1079–1092

Shannon P, Markiel A, Ozier O, Baliga NS, Wang JT, Ramage D, Amin N, Schwikowski B, Ideker T (2003) Cytoscape: a software environment for integrated models of biomolecular interaction networks. Genome Res **13**: 2498–2504

Shen JR (2015) The structure of photosystem II and the mechanism of water oxidation in photosynthesis. Annu Rev Plant Biol **66**: 23–48

Srere PA (1985) The metabolon. Trends Biochem Sci **10**: 109–110

Srere PA (1987) Complexes of sequential metabolic enzymes. Annu Rev Biochem **56**: 89–124

Srere PA, Mattiasson B, Mosbach K (1973) An immobilized three-enzyme system: a model for microenvironmental compartmentation in mitochondria. Proc Natl Acad Sci USA **70**: 2534–2538

Stellberger T, Häuser R, Baiker A, Pothineni VR, Haas J, Uetz P (2010) Improving the yeast two-hybrid system with permutated fusions proteins: the Varicella Zoster Virus interactome. Proteome Sci **8**: 8

Ströher E, Grassl J, Carrie C, Fenske R, Whelan J, Millar AH (2016) Glutaredoxin S15 is involved in Fe-S cluster transfer in mitochondria influencing lipoic acid-dependent enzymes, plant growth, and arsenic tolerance in Arabidopsis. Plant Physiol **170**: 1284–1299

Sumegi B, Srere PA (1984a) Binding of the enzymes of fatty acid beta-oxidation and some related enzymes to pig heart inner mitochondrial membrane. J Biol Chem **259**: 8748–8752

Sumegi B, Srere PA (1984b) Complex I binds several mitochondrial NAD-coupled dehydrogenases. J Biol Chem **259**: 15040–15045

Sweetlove LJ, Beard KF, Nunes-Nesi A, Fernie AR, Ratcliffe RG (2010) Not just a circle: flux modes in the plant TCA cycle. Trends Plant Sci **15**: 462–470

Thimm O, Bläsing O, Gibon Y, Nagel A, Meyer S, Krüger P, Selbig J, Müller LA, Rhee SY, Stitt M (2004) MAPMAN: a user-driven tool to display genomics data sets onto diagrams of metabolic pathways and other biological processes. Plant J **37**: 914–939

Van Leene J, Eeckhout D, Persiau G, Van De Slijke E, Geerinck J, Van Isterdael G, Witters E, De Jaeger G (2011) Isolation of transcription factor complexes from Arabidopsis cell suspension cultures by tandem affinity purification. Methods Mol Biol **754**: 195–218

Vélot C, Mixon MB, Teige M, Srere PA (1997) Model of a quinary structure between Krebs TCA cycle enzymes: a model for the metabolon. Biochemistry **36**: 14271–14276

Wang C, Marshall A, Zhang D, Wilson ZA (2012) ANAP: an integrated knowledge base for Arabidopsis protein interaction network analysis. Plant Physiol **158**: 1523–1533

Winkel BS (2004) Metabolic channeling in plants. Annu Rev Plant Biol **55**: 85–107

Winzer T, Kern M, King AJ, Larson TR, Teodor RI, Donninger SL, Li Y, Dowle AA, Cartwright J, Bates R, (2015) Morphinan biosynthesis in opium poppy requires a P450-oxidoreductase fusion protein. Science **349**: 309–312

Wiśniewski JR, Zougman A, Nagaraj N, Mann M (2009) Universal sample preparation method for proteome analysis. Nat Methods **6**: 359–362

Wu F, Minteer S (2015) Krebs cycle metabolon: structural evidence of substrate channeling revealed by cross-linking and mass spectrometry. Angew Chem Int Ed Engl **54**: 1851–1854

Wu FH, Shen SC, Lee LY, Lee SH, Chan MT, Lin CS (2009) Tape-Arabidopsis Sandwich: a simpler Arabidopsis protoplast isolation method. Plant Methods **5**: 16

Zhang Q, Marsolais F (2014) Identification and characterization of omega-amidase as an enzyme metabolically linked to asparagine transamination in Arabidopsis. Phytochemistry **99**: 36–43

Zhang Y, Beard KFM, Swart C, Bergmann S, Krahnert I, Nikoloski Z, Graf A, Ratcliffe RG, Sweetlove LJ, Fernie AR, (2017a) Protein-protein interactions and metabolite channelling in the plant tricarboxylic acid cycle. Nat Commun **8**: 15212

Zhang Y, Sun H, Zhang J, Brasier AR, Zhao Y (2017b) Quantitative assessment of the effects of trypsin digestion methods on affinity purification-mass spectrometry-based protein-protein interaction analysis. J Proteome Res **16**: 3068–3082